Geochemistry Geophysics Geosystems G3

Article
Volume 13, Number 1
21 July 2012
Q0AK07, doi:10.1029/2012GC004056
ISSN: 1525-2027

Published by AGU and the Geochemical Society

Evolutionary aspects of lithosphere discontinuity structure in the western U.S.

Alan Levander
Department of Earth Science, Rice University, MS-126, 6100 Main Street, Houston, Texas 77005, USA (alan@rice.edu)

Meghan S. Miller
Department of Earth Sciences, University of Southern California, Zumberge Hall of Science, 3651 Trousdale Parkway, Los Angeles, California 90089-0740, USA

[1] We have produced common conversion point (CCP) stacked Ps and Sp receiver function image volumes of the Moho and lithosphere-asthenosphere boundary (LAB) beneath the western United States using Transportable Array data. The large image volumes and the diversity of tectonic environments they encompass allow us to investigate evolution of these structural discontinuities. The Moho is a nearly continuous topographic surface, whereas the LAB is not and the seismic images show a more complex expression. The first order change in LAB depth in the western U.S. occurs along the Cordilleran hingeline, the former Laurasian passive margin along the southwestern Precambrian North American terranes. The LAB is about 50% deeper to the east of the hingeline than to the west, with most of the increase in LAB thickness being in the mantle lithosphere. We infer that the Moho and the LAB are Late Mesozoic or Cenozoic everywhere west of the hingeline, modified during Farallon subduction and its aftermath. Between the hingeline and the Rocky Mountain Front, the LAB, and to a lesser extent the Moho, have been partially reset during the Cenozoic by processes that continue today. Seismicity and recent volcanism in the interior of the western U.S. are concentrated along gradients in crustal and/or lithospheric thickness, for example the hingeline, and the eastern edge of the coastal volcanic-magmatic terranes. To us this suggests that lateral gradients in integrated lithospheric strength focus deformation. Similarly, areas conjectured to be the sites of convective downwellings and associated volcanism are located along gradients in regional lithosphere thickness.

Components: 12,400 words, 7 figures, 5 tables.

Keywords: Moho; lithosphere-asthenosphere boundary; western U.S.

Index Terms: 7218 Seismology: Lithosphere (1236); 8110 Tectonophysics: Continental tectonics: general (0905).

Received 18 January 2012; **Revised** 31 May 2012; **Accepted** 6 June 2012; **Published** 21 July 2012.

Levander, A., and M. S. Miller (2012), Evolutionary aspects of lithosphere discontinuity structure in the western U.S., *Geochem. Geophys. Geosyst.*, *13*, Q0AK07, doi:10.1029/2012GC004056.

Theme: The Lithosphere-Asthenosphere Boundary

1. Introduction

[2] The strong, largely coherent outer layer of the Earth, the lithosphere, that translates over a weaker layer, the asthenosphere, is a fundamental plate tectonic concept that forms part or all of the outer chemical, mechanical, and thermal boundary layer(s) of the convecting mantle, depending on which geoscientist's definition of lithosphere is considered. The half-space cooling model defines the thermal boundary layer of the oceanic lithosphere, predicting an increasing lithosphere thickness with age, and therefore an increasing depth to the lithosphere-asthenosphere boundary (LAB) with age. An alternate definition is that the LAB is a compositional boundary between chemically depleted peridotite in the lithosphere and fertile, hydrated peridotite in the asthenosphere with the result that, in the authors' words, "the location of the thermal boundary layer is strongly influenced by a compositional boundary" [*Hirth and Kohlstedt*, 1996]. On the vastly older continents, lithospheric thickness has been negatively correlated with heat flow and the age of last tectono-magmatic, or orogenic event [*Artemieva*, 2009; *Chapman and Pollack*, 1977; *Lee*, 2006; *Lee et al.*, 2005; *Sleep*, 2005], and is thought in some places to be a boundary between dehydrated mantle minerals whose water was removed during melt extraction and more fertile hydrated peridotite. The thickness of the lithosphere, and hence the depth to the LAB, is currently under investigation, as is how it is geodynamically modified over time [*Eaton et al.*, 2009; *Fischer et al.*, 2010; *Kawakatsu et al.*, 2009; *Rychert and Shearer*, 2009; *Abt et al.*, 2010; *Miller and Eaton*, 2010].

[3] The oceanic Moho, once formed, is a stable boundary until the oceanic plate subducts, which subjects the basaltic oceanic crust to a rapidly changing stress field and increasing P-T conditions, which decreases or even reverses the sign of the velocity contrast with the underlying depleted peridotite mantle through dehydration and eclogitization of the crust [*Bostock et al.*, 2001, 2002; *Rondenay et al.*, 2001]. In contrast, in the more complicated continental system the Moho can be tectonically, magmatically, or metamorphically reset [*Cook et al.*, 2010; *Griffin and O'Reilly*, 1987; *Jarchow and Thompson*, 1989; *Klemperer et al.*, 1986]. Even using the strict seismic definition of the Moho as that depth at which P velocity abruptly increases to 7.6 km/s or greater, the meaning of the continental Moho can be quite variable in terms of structure, lithology, and mineralogy. *Cook et al.* [2010] provide a good overview. By definition a geophysical boundary, the Moho typically is closely correlated with a change in chemistry, and hence mineralogy and lithology, from crustal to mantle compositions. It has also been argued that in places the Moho represents a metamorphic phase change rather than a chemical boundary [*Griffin and O'Reilly*, 1987].

[4] Although these two prominent continental lithospheric discontinuities can be altered with time as a result of tectonic processes, prior to the deployment of large 3D broadband seismic arrays seismic data were not available for examining discontinuity variations systematically throughout an entire orogen. The EarthScope USArray facility (Figure 1) makes the western U.S. orogenic plateau an exceptional natural laboratory in which to examine lithosphere modification over time since deformation has been ongoing from the late Mesozoic through the present, and has largely resulted from processes associated with Farallon plate subduction beneath North America and its immediate aftermath. A few of the most important of these episodes are: (1) the formation of the Sierra Nevada and other batholiths in the Mesozoic and early Cenozoic; (2) the formation of the Sevier fold and thrust belt; (3) a possible Andean style orogenic plateau, the "Nevadoplano" [*DeCelles*, 2004]; (4) the Laramide uplifts associated with Farallon flat slab subduction; (5) Farallon removal and the ignimbrite "flare-up" [*Humphreys*, 1995]; (6) Basin and Range extension; (7) and the cessation of subduction and initiation of transform motion that began in the Oligocene and has now encompassed more than half of the western continental margin of the conterminous U.S. [*Atwater*, 1970]. A number of authors have suggested that significant deformation has resulted from processes that are major perturbations on the plate tectonic model, with secondary convection playing an important role in the back-arc, following slab removal, and during post-orogenic collapse [*Humphreys*, 1995; *Humphreys et al.*, 2003; *Hyndman et al.*, 2005; *Karlstrom and Humphreys*, 1998; *Levander et al.*, 2011; *Smith et al.*, 1989; *Zandt and Humphreys*, 2008], in keeping with the characterization of the region from the SAF to the Rocky Mountain front as a diffuse plate boundary zone [*Gordon*, 1998].

[5] In this paper we examine the two lithospheric discontinuities in the western U.S. (Figures 2–6) attempting to relate their current configurations to North American plate boundary evolution in the Mesozoic and Cenozoic. The first order lithospheric structure suggests that variations in lithospheric strength focus deformation, which appears to act as

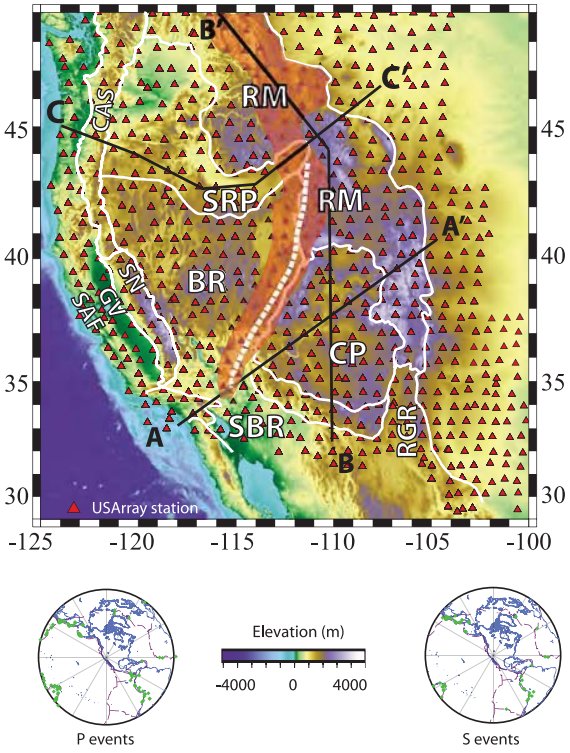

Figure 1. (top) Map of the USArray Transportable Array stations used in the receiver function analysis. The tectonic/physiographic boundaries are represented by thick white lines. The white dashed line is the location of the Cordilleran hingeline marking the edge of the North American Paleozoic passive margin, and the locus of the Sevier orogeny (red shading). Black solid lines are receiver function profiles shown in Figure 2. SAF: San Andreas Fault and Coastal Ranges, CAS: Cascadia Range, SN: Sierra Nevada Range, SRP: Snake River Plain, RM: Rocky Mountains, BR: Basin and Range, CP: Colorado Plateau, RGR: Rio Grande Rift. (bottom) The azimuthal distribution of the events used in the Ps and Sp receiver functions.

a positive feedback as lithospheric modifications caused by deformation then enhance deformation (Figures 6 and 7). As we describe below, the systematically well-sampled Moho and LAB depth estimates (Figure 3) presented suggest that since the onset of Farallon subduction the Moho and LAB have been reset almost everywhere west of the Cordilleran hinge-line, i.e., the Paleozoic Laurasian passive margin and later the locus of Sevier belt deformation. Between the hinge-line and the Rocky Mountain front, depending on locale, these lithospheric discontinuities have undergone a range of dynamic modifications, from significant to minimal. In the regions along and east of the hinge-line, modern convective processes and associated magmatism are deforming the continental edges, with deformation sometimes localized on Precambrian sutures, inherited from continental construction in the Paleoproterozoic [*Karlstrom and Humphreys*, 1998]. As described in a number of papers [*Forsyth and Rau*, 2009; *Lonsdale*, 1991; *Meltzer and Levander*, 1991; *Schmandt and Humphreys*, 2011], Farallon plate fragments still reside in the upper mantle in various places across the orogen, complicating the lithospheric and upper mantle structure.

2. Data and Methodology

[6] Using data from the EarthScope USArray Transportable Array we have produced Ps and Sp receiver functions to recover the converted wave response beneath each USArray station in the western U.S. (Figure 1). For both Ps and Sp receiver functions, we first rotated ZNE into ZRT, and then rotated ZRT into LQT [*Vinnik*, 1977] using the incidence angles predicted by AK135 [*Kennett et al.*, 1995]. In the case of Ps receiver functions the direct vertical and L (longitudinal) component was deconvolved from the radial and in-plane S

Figure 2. CCP cross sections through (a, c, and e) the Ps receiver function volume and (b, d, and f) the Sp receiver function volume along the profiles shown in Figure 1. Black arrows indicate bends in cross-sections. The data are normalized with red positive amplitudes, and blue negative (see text). The Moho is shown by black symbols, circles for the Ps continuity picks, black triangles from H-k analysis. The differences between the Sp and Ps Moho continuity picks are negligible (Table 1). The arrival of the first crustal multiple in the Ps section is shown as a dashed black line. The LAB picked by continuity is shown by white symbols, circles for Ps, triangles for Sp. The Ps LAB chosen for conformity to Sp is shown as a white dashed line. A-A′ shows Moho and LAB complications beneath the Colorado Plateau, along the southeastern edge of a delaminating region (see text). In B-B′ the Moho is offset (top to the north) at the Cheyenne belt (right red arrow) along the northern edge of the Colorado Plateau, congruent with a putative north-dipping ancient slab frozen into the Paleoproterozoic-Archean suture observed by *Yuan and Dueker* [2005]. The LAB deepens under the CP and RM in both cross-sections, particularly under the RM north of the CP, with complications under Yellowstone (Y). Along B-B′, LAB depth under the CP agrees with an upper mantle low velocity zone identified by Deep Probe (left red arrow, see auxiliary material) [*Gorman et al.*, 2002; *Henstock et al.*, 1998; *Snelson et al.*, 1998]. Profile C-C′ shows mild upper mantle complications in the Cascadia backarc region, and significant complications under Yellowstone (Y), but overall shows good agreement between Ps and Sp LAB picks.

motion, respectively; for Sp, rotated Q was deconvolved from the longitudinal L motion. Teleseismic Ps receiver functions are higher frequency (0.5–2 Hz) than Sp, which are made with an upper frequency of 0.1–0.2 Hz, and therefore have about an order of magnitude better resolving power. Ps receiver functions are excellent for identifying the Moho and large crustal features but can suffer from strong crustal multiple reflections following the direct P arrival by ~12–25 s, depending upon crustal thickness (see Figure S1 in Text S1 in the auxiliary material), thereby interfering with conversions from the upper mantle.[1] Although teleseismic Sp receiver functions are lower in frequency they do not suffer from multiple contamination as converted P phases are precursors to S. The converted Sp-wave paths are considerably longer and more oblique than the converted Ps paths [*Yuan et al.*, 2006] and are therefore more subject to errors in space-depth positioning during CCP stacking. Since Sp receiver functions use converted P waves whose wavelengths are ~5–10 times greater than the converted S-waves in Ps receiver functions (~f_{Ps}/f_{Sp}*1.75), Sp rarely resolve intracrustal structure, but can be used for determining Moho depth, and are excellent for detecting relatively broad vertical gradients in velocity, such as might be expected for a thermally controlled LAB [*Eaton et al.*, 2009]. The combination of both types of receiver functions allow for independent discontinuity models of the same area in different frequency bands using converted waves having very different raypaths. The two models, however, are coupled through the velocity model used for depth imaging.

[7] Here we present the results from two 3D image volumes, one made of ~11,000 Ps and one made of ~5,000 Sp receiver functions both from 556 TA stations. The image volumes extend from the Pacific coast to the Great Plains east of the Rocky Mountain front, and between the U.S. borders with Mexico and Canada. Ps receiver functions were made from 106 well recorded earthquakes in the distance range $35° < \Delta < 90°$; the Sp receiver functions were made from 57 well recorded earthquakes at $55° < \Delta < 85°$; the data were recorded at USArray stations from 2005 to 2009 (Figure 1). We rejected more events than we kept for analysis due to low signal-to-noise ratios.

[8] The image volumes were constructed by first hand editing the seismograms, then producing and hand editing the receiver functions, then mapping the converted wave signals from time to space, station by station, for each earthquake, and finally summing all the individual event images. We produced the Ps receiver functions in several different frequency bands using both frequency domain [*Langston*, 1977] and iterative time domain [*Ligorria and Ammon*, 1999] methods. For Ps we made RFs with maximum frequencies of 2.0, 1.0, and 0.5 Hz, deconvolving both the vertical from the radial and the longitudinal component from the in-plane S component. Extensive comparisons show that iterative deconvolution and spectral division with water level damping produce similar results. As a form of quality assurance we rejected RFs for which the frequency domain and iterative deconvolution results were inconsistent.

[9] For Sp we made RFs with 0.4, 0.2, 0.1, and 0.05 Hz upper frequencies, deconvolving Q from the L component using the frequency domain water level deconvolution, iterative time domain deconvolution, and a newly developed least squares inverse filtering deconvolution method which we describe elsewhere [see *Robinson and Treitel*, 1980]. Quality control was provided by comparing the receiver functions from different methods, with the least square inverse filtering arguably producing the highest quality Sp RFs.

[10] Here we show 0.5 Hz Ps and 0.2 Hz Sp receiver functions, the former made by time domain iterative deconvolution, the latter by least squares inverse filtering. We also reverse the polarity of the Sp signals for comparison with the Ps images in which red denotes a positive impedance contrast with depth (as in the Moho conversion). We deliberately chose a relatively low frequency for the Ps receiver functions for this study, as our goal is to estimate the province-wide character of the Moho and LAB, rather than local Moho irregularities [*Larkin et al.*, 1997; *Cook et al.*, 2010]. The thermal

[1] Auxiliary materials are available in the HTML. doi:10.1029/2012GC004056.

Figure 3. Maps showing the depth below sea level to (a) Moho estimated from Ps receiver functions, (b) Moho estimated from Sp receiver functions, (c) LAB interpreted from the Ps receiver functions, (d) LAB interpreted from the Sp receiver functions, and (e) the LAB interpreted using the Sp RFs as a guide east of the Sevier Thrust (ST). The latter is nearly identical to Figure 3c west of the Sevier Thrust and to Figure 3d to the east. The thick black lines are physiographic/tectonic boundaries as in Figure 1, black dashed line is the Sevier Thrust belt (ST), white dashed lines are age boundaries, CB is Cheyenne Belt. South of the Cheyenne Belt terranes are Paleo-Proterozoic and younger. North of CB is the Archean Wyoming Province. Y is Yellowstone (see Tables 1–4).

Table 1. Moho Depths: Ps and Sp

	Ps Moho Depth	Sp Moho Depth	Difference Sp-Ps
Sierra Nevada	39.4 ± 2.9	38.0 ± 2.8	−1.4
Cascades	39.6 ± 3.4	36.8 ± 4.8	−2.8
Basin and Range	35.6 ± 5.0	33.8 ± 4.0	−1.8
Northern Basin and Range	36.3 ± 3.6	34.4 ± 3.0	−1.9
Southern Basin and Range and Rio Grande Rift	33.5 ± 7.2	31.9 ± 5.4	−1.6
Snake River Plain	39.3 ± 3.5	38.2 ± 3.4	−1.1
Rocky Mountains	43.3 ± 5.7	44.1 ± 5.8	0.8
Colorado Plateau	43.4 ± 5.3	42.8 ± 5.9	−0.6
Western U.S.	38.6 ± 6.8	37.2 ± 8.0	−1.4

varying, i.e., 1D velocity model, AK135 [*Kennett et al.*, 1995]. This process is termed seismic migration by some authors. CCP processing does not restore dipping events or collapse diffractions, which is the common definition of migration processing in exploration seismology [see *Rondenay*, 2009]. We corrected for 3D velocity perturbations along the 1D raypaths using the linear tomography assumption with the travel time corrections calculated from a hybrid 3D velocity model. We constructed this model by smoothly merging the Crust2.0 velocities [*Bassin et al.*, 2000; *Mooney et al.*, 1998], with an uppermost mantle Vp model [*Buehler and Shearer*, 2010] and then blending that with the deeper finite-frequency Vp and Vs tomography mantle models at depths >60 km [*Schmandt and Humphreys*, 2010]. We calculated the Fresnel zone in 3D for each P-S ray pair for each depth empirically by comparing P and S travel times for paths around the specular ray. T/2 is the null of the first Fresnel zone for waves of period, T, taken as twice the period of the Gaussian shaping filter used in the RF calculation (i.e., 4 s for Ps and 10 s for Sp). The amplitude mapped to a particular depth along the specular ray was spread over the first Fresnel zone using a 2D tapered function having unit amplitude at the specular ray conversion point and decreasing linearly to zero at the edge of the Fresnel zone function. The shape of the Fresnel zone can be seen in the hitcount plots in Figure S3 in Text S1. Given the 70 km TA station spacing, the Ps Fresnel zones in the depth range 1–180 km vary from non-overlapping to slightly overlapping due to the steep incidence angle of the converted S wave and the 0.5 Hz upper cutoff frequency used in processing the RFs (Figure S3 in Text S1). To make continuous images the final Ps CCP stacked volume was smoothed using a 2D Gaussian weighting filter whose width was approximately that of the USArray station spacing (∼70 km). The Sp receiver functions were made with lower frequency waves, f ≤ 0.2 Hz, with more oblique incidence angles, and therefore considerably larger Fresnel zones. Even at 70 km station spacing, the Fresnel zones of Sp signals overlap at virtually all depths (Figure S3 in Text S1). No smoothing of the Sp CCP stacks other than the Fresnel zone weighting was required. As a further form of quality assurance we made bootstrap calculations on both the Ps and Sp receiver gathers at every USArray station to assess the variance in the receiver gathers and the CCP gathers. We did 10^4 bootstrap iterations with replacement on the moveout corrected receiver functions. A random selection of gathers is shown in Figure S4 in Text S1. We then repeated this, doing 10^4 bootstrap iterations with replacement on the unstacked Ps and Sp image volumes for every CCP location beneath a USArray station (Figure S5 in Text S1). In both cases the variance is considerably smaller than the mean, as we show in Figure 4, giving us confidence that the Moho and LAB signals are robust.

[12] Moho depths were determined two ways: 1) For Ps and for Sp we followed image continuity in the image volumes along every constant longitude and every constant latitude profile, producing two grids for each CCP volume, each with 0.25° intervals. The two grids were then averaged. (This results in the hand picked surface not coinciding exactly with the maximum value on the CCP sections on profiles at some azimuths). The Ps and Sp estimates of Moho depth are generally within a few kilometers of one another (Table 1), with the Sp values being almost uniformly shallower, as predicted by the modeling described in the auxiliary material. 2) We also determined Ps Moho depth and the Vp-Vs ratio at 431 of the 502 USArray stations using the H-κ method of *Zhu and Kanamori* [2000]. We could not determine a stable measurement at 71 stations. We found the H-κ estimates of Moho depth using the Crust2.0 Vp model are generally less than those we determined

Table 2. Moho Depths: Ps and H-κ

	Ps Moho Depth	Ps H-κ Moho Depth	Difference Ps-H
Sierra Nevada	39.4 ± 2.9	36.9 ± 4.9	2.5
Cascades	39.6 ± 3.4	35.3 ± 4.0	3.5
Basin and Range	35.6 ± 5.0	30.2 ± 3.5	5.4
Northern Basin and Range	36.3 ± 3.6	30.3 ± 2.9	6.0
Southern Basin and Range and Rio Grande Rift	33.5 ± 7.2	29.5 ± 4.8	4.0
Snake River Plain	39.3 ± 3.5	36.0 ± 4.0	3.3
Rocky Mountains	43.3 ± 5.7	38.2 ± 4.7	5.1
Colorado Plateau	43.4 ± 5.3	37.1 ± 4.9	6.3
Western U.S.	38.6 ± 6.8	33.9 ± 5.8	4.7

from the CCP image volumes, the difference averaging 4.7 km (Table 2). We found that the differences were spread rather uniformly across the entire western U.S. (see Figure 2). Vp/Vs from the H−κ analysis averaged 1.75 ± 0.04. We note that very similar Moho maps to the ones we have produced have already been published by other researchers using Ps receiver functions [*Gilbert*, 2012; *Lowry and Pérez-Gussinye*, 2011].

[13] The depth to the LAB was determined by individually and separately examining the Sp and Ps image volumes with shear velocity models from Rayleigh wave analysis where available [*Liu et al.*, 2011, 2012; *Yang et al.*, 2008]. To avoid confusing crustal multiples with primary signals in the Ps image volumes, we generated Haskell matrix synthetic seismograms using both Moho models (continuity and H-κ) for each USArray receiver using the Crust2.0 velocity model, creating image volumes of these to identify the crustal multiples (see Figure S1 in Text S1). The synthetic sections were also used for identifying intracrustal events and basin reverberations. As for the Moho, LAB depths were picked on every constant longitude profile and every constant latitude profile and the resulting two grids were averaged. The first set of LAB determinations were made by choosing the first continuous negative event beneath the Moho individually on the Ps and Sp CCP volumes. For LAB depths less than about 70 km, which includes most of the terranes west of the Cordilleran hingeline, the Ps and Sp depths picked in this way compare well (Table 3). For the greater LAB depths beneath the Colorado Plateau and Rocky Mountains the first negative sub-Moho Ps signal is significantly shallower, 16–22 km (see Table 3) than the first negative Sp signal. For the Rockies and Colorado Plateau we therefore also picked a Ps LAB as the nearest negative event conforming to the Sp LAB depth. This significantly improved agreement between the two data sets under the Colorado Plateau and Rocky Mountains, giving differences comparable to the other terranes (Table 4). This does mean that we are imaging unexplained strong negative events in the upper mantle lithosphere (see Figure S2b in Text S1). We discuss this further below.

3. Results

[14] We illustrate the data used for Moho and LAB depths with a few representative cross sections from the Ps and Sp image volumes. The full image volumes are available at the IRIS DMS and in the auxiliary material. Cross section A-A′ (Figures 2a and 2b) extends from the Pacific across the

Table 3. LAB Depths: First Negative Below Moho

	Ps LAB Depth	Sp LAB Depth	Difference Sp-Ps
Sierra Nevada	66.9 ± 6.0	67.8 ± 1.9	0.9
Cascades	60.3 ± 6.0	66.9 ± 7.1	6.6
Basin and Range	59.9 ± 8.7	66.1 ± 9.3	6.2
Northern Basin and Range	60.3 ± 7.1	65.4 ± 9.4	5.1
Southern Basin and Range and Rio Grande Rift	58.4 ± 11.9	65.1 ± 8.9	6.7
Snake River Plain	63.7 ± 5.7	70.4 ± 14.3	6.7
Rocky Mountains	70.7 ± 9.8	92.6 ± 18.9	21.9
Colorado Plateau	77.0 ± 10.3	92.8 ± 15.2	15.8
Western U.S.	64.7 ± 11.4	76.1 ± 18.7	11.4

Table 4. LAB Depths: Ps Conformity With Sp

	Ps LAB Depth	Sp LAB Depth	Difference Sp-Ps
Sierra Nevada	66.9 ± 6.0	67.8 ± 1.9	0.9
Cascades	60.3 ± 6.0	66.9 ± 7.1	6.6
Basin and Range	61.8 ± 9.3	66.1 ± 9.3	4.3
Northern Basin and Range	60.7 ± 7.8	65.4 ± 9.4	4.7
Southern Basin and Range and Rio Grande Rift	62.3 ± 12.1	65.1 ± 8.9	2.8
Snake River Plain	67.3 ± 12.5	70.4 ± 14.3	3.1
Rocky Mountains	91.5 ± 19.4	92.6 ± 18.9	1.1
Colorado Plateau	86.2 ± 13.9	92.8 ± 15.2	6.6
Western U.S.	72.1 ± 19.7	76.1 ± 18.7	4.0

southern Basin and Range, the Colorado Plateau, and the Rocky Mountains to the Great Plains, showing the difference in character of the Ps and Sp images, as well as examples of the complexity of western U.S. lithospheric structure. On this cross-section, the Moho and LAB generally are shallowest in the coastal regions, and beneath the Basin and Range (see Figure 3). They deepen beneath the Colorado Plateau and the Rocky Mountains. The Moho shows complexity under the Colorado Plateau, which we discuss further below, and on this profile, is relatively featureless beneath the Rocky Mountains. The difference between the continuity picks and the H-κ Moho depth determinations is clear on this section, and is representative of the western U.S. generally. LAB depths chosen as the first negative event beneath the Moho coincide for Ps and Sp beneath the southern Basin and Range at 40–60 km depth, and differ beneath parts of the Colorado Plateau and Rocky Mountains. A second equally strong and nearly as continuous event under the southern Basin and Range is visible on the Ps section at about 75 km depth, an observation reported for Sp LAB signals in Southern California and the Salton Trough [*Lekic et al.*, 2011]. A summary of average LAB depths and their standard deviations for each physiographic province is given in Tables 3 and 4.

[15] Cross section B-B′ (Figures 2c and 2d) shows the structure of the southern Basin and Range, the Colorado Plateau and the axis of the Rocky Mountains. The Moho is shallow beneath the southern Basin and Range (~33 km) and deepens to more than 40 km beneath the Colorado Plateau and Rocky Mountains, undulating from the central Colorado Plateau (~37°N) to the Yellowstone region (~44–45°N). Near the Cheyenne Belt, the crust appears to be overthrust from the north. This cross section illustrates where the Ps continuity LAB depths (first negative beneath Moho), and the Sp LAB depths are in greatest disagreement, on average 21.9 km beneath the Rockies and 15.8 km beneath the Colorado Plateau (white arrows). Using the Sp as a guide provides consistent Ps and Sp LAB depths, but does result in strong continuous negative Ps events within the lithospheric mantle. Also note the strong positive amplitude events in the Sp cross section below the crust beneath the Yellowstone region and northward.

[16] The third cross section, C-C′ (Figure 2e and 2f), extends from the Cascadia subduction zone across the Cascade volcanoes, the High Lava Plains, along the axis of the Snake River Plain to Yellowstone and across the Rocky Mountains. The Moho and LAB are relatively flat from the Cascades to Yellowstone where they abruptly deepen under the Rockies. The subducting Juan de Fuca Plate is partially visible on the western end of the profile. The LAB signals are somewhat complicated under the Cascades, and also under the transition to the Rockies across Yellowstone (white arrows). The continuity Ps and Sp LAB depths differ significantly only at the province boundary, which can be resolved by using Sp as a guide. Note that there are strong deep positive Sp conversions well below crustal depths under the Yellowstone region. Moho depths are generally in good agreement with a number of active source studies as are the LAB depth estimates from active source data along the PACE and DeepProbe profiles [*Gorman et al.*, 2002; *Henstock et al.*, 1998; *Holbrook*, 1990; *Levander et al.*, 2005; *Parsons et al.*, 1996; *Snelson et al.*, 1998] as shown in Figure S6 in Text S1.

[17] We also calculated amplitude ratios for the Moho and LAB conversions from the image volumes at the depths picked for the Moho and LAB. This forms two more surfaces for each volume, from which we determined the amplitude ratios of the Moho to LAB signals (Table 5). In the case of the Ps RFs, we can also reference the Moho amplitude to the direct P wave. The average Ps and

Table 5. Amplitudes

	A_{Ps}(Moho)/A_P	A_{Ps}(Moho)/A_{Ps}(LAB) First Negative	A_{Ps} (Moho)/A_{Ps} (LAB) Conformity	A_{Sp}(Moho)/A_{Sp}(LAB) Ratio
Sierra Nevada	0.16 ± 0.07	−2.2 ± 1.3	−2.2 ± 1.3	−2.4 ± 1.7
Cascades	0.16 ± .10	−1.4 ± 0.8	−1.4 ± 0.8	−1.8 ± 0.9
Basin and Range	0.20 ± 0.08	−2.0 ± 0.9	−2.1 ± 1.0	−2.7 ± 1.6
Northern Basin and Range	0.20 ± 0.08	−2.0 ± 0.9	−2.1 ± 1.0	−2.4 ± 1.6
Southern Basin and Range and Rio Grande Rift	0.20 ± 0.08	−2.0 ± 0.9	−2.2 ± 1.1	−3.2 ± 1.7
Snake River Plain	0.15 ± 0.08	−1.9 ± 0.9	−1.9 ± 0.9	−3.6 ± 1.7
Rocky Mountains	0.15 ± .07	−2.1 ± 1.2	−2.4 ± 1.5	−2.50 ± 2.0
Colorado Plateau	0.11 ± 0.04	−2.4 ± 1.4	−2.4 ± 1.5	−1.8 ± 1.0
Western U.S.	0.16 ± 0.08	−2.1 ± 1.1	−2.2 ± 1.3	−2.5 ± 1.7

Sp amplitude ratios are generally comparable within each province although some have fairly large variations within a province (see Figure 5). The exceptions to this are the Snake River Plain/Columbia Plateau and the southern Basin and Range, where Sp is more than 50% larger than Ps (see Table 5). The Snake River Plain/Columbia plateau shows low Sp ratios in the Cascadia backarc region with more normal values in the Snake River Plain proper. The southern Basin and Range province has the thinnest crust and lithosphere, therefore the likelihood for Sp interference is greatest, making the amplitude ratios less reliable. For the entire western U.S. the Moho/LAB amplitude ratio is −2.1 ± 1.1 to −2.2 ± 1.3 for Ps and −2.5 ± 1.7 for Sp. Translated to an impedance ratio, this suggests that on average, the LAB impedance contrasts are 40–50% that of the Moho. The averages of amplitude ratios from province to province vary from a low of −1.4 to a high of −3.6, suggesting the contrasts in impedance at the LAB vary from about 70% to less than 30% that at the Moho (Table 5).

4. Interpretations

4.1. Moho

[18] The Moho map we present agrees reasonably well with Moho maps produced previously using USArray Ps receiver functions [*Gilbert*, 2012; *Lowry and Pérez-Gussinye*, 2011]. *Lowry and Pérez-Gussinye* [2011] provide an interesting tectonic interpretation of regional Vp-Vs ratio and the relation to estimated elastic plate thickness. *Gilbert* [2012] provides a detailed province by province interpretation of crustal structure. We make a few additional observations about Moho structure. The interpretation of the Moho as a chemical boundary works well in most of the western U.S., although without implying common origin by this statement. The Moho has only a few localized interruptions (Figure 3), such as above the front of the mantle wedge in parts of the Cascadia forearc where the upper mantle has been serpentinized [*Blakely et al.*, 2005; *Bostock et al.*, 2002; *Brocher et al.*, 2003; *Liu et al.*, 2012] and in the western and northern Great Valley where the Coast Range ophiolite occupies a significant part of the crust and is also serpentinized [*Godfrey et al.*, 1997]. Although CCP stacking blurs dipping features, we can identify the Moho of the subducting oceanic crust in the Juan de Fuca plate to approximately 60 km depth in parts of Cascadia. (Our Moho map does not show the Juan de Fuca oceanic Moho, as it is not continuous with the western U.S. lithosphere). The amplitude analysis indicates that the Ps Moho conversion is strong in much of the Basin and Range with the stronger Moho signals correlated with thinner crust found across the northern Basin and Range at about 40°N and particularly under the Great Salt Lake. Among the thinnest crust in the western U.S. is along the axis of the Salton Trough, which stands out on both the Ps and Sp Moho depth maps, where Moho depth varies from ∼28 km to as little as ∼25 km.

[19] With a few isolated exceptions, the Moho conversion is relatively weak along most of the Sierra Nevada and Cascades, under most of the Rocky Mountains, Colorado Plateau and Rio Grande Rift (Figure 2a). It varies in strength between being weak and strong in the Cascadia backarc region (Figure 4). Where local convective downwelling/delamination events have been identified, the Moho structure is complicated and the amplitude is locally weak, for example beneath the Wallowa Mountains [*Hales et al.*, 2005], parts of the Sierra Nevada (Figures 5a and 5b; see also Figure S4e in Text S1 in the auxiliary material) [*Zandt et al.*, 2004], and

the west-central Colorado Plateau (Figures 2a and 2b) [see also *Levander et al.*, 2011, Figure 3].

4.2. Lithosphere-Asthenosphere Boundary

[20] In some areas the upper mantle has LAB signals in both of the receiver function image volumes that are long and continuous like the Moho, while in other places they are discontinuous and quite complex, which is much less like the Moho (Figures 2 and 5). West of the hingeline the Ps and Sp depths generally agree in depth within the variations observable within a given province, east of the hingeline, the same can be said of the Sp and conformity Ps LAB (Tables 3 and 4). Regions of LAB complexity appear under some of the province boundaries, and particularly those with the Rockies and Colorado Plateau.

[21] It is worth reviewing the possible causes of complexity in the seismically observed LAB. The lithosphere-asthenosphere boundary sensu stricto is defined rheologically as the zone dividing the mantle that translates with the plate, and mantle that takes part in convection [*Eaton et al.*, 2009; *Fischer et al.*, 2010], i.e., it is the convective sublayer [*Lee et al.*, 2005] at the base of the upper boundary layer of the convecting mantle. Thermally, it is defined as the depth range in which the conductive geotherm intersects the mantle adiabat. The seismic LAB is an attempt to correlate an observed seismic velocity reduction that is thermally, chemically, and/or grain-size controlled with the rheological / thermal LAB, e.g., base of a high velocity mantle lid over a lower velocity asthenosphere [*Farra and Vinnik*, 2000; *Kawakatsu et al.*, 2009; *Li et al.*, 2007; *Rychert et al.*, 2007; *Yuan et al.*, 2006].

[22] This view has the virtue of simplicity, but masks the geologic complexity that is possible in an active orogen, which can be outlined by reviewing the sources of the velocity reduction at the LAB. This has been ascribed to: 1) variation in chemistry from a partially depleted harzburgite to a more fertile mantle with depth, coincident with a change in thermal gradient from conduction to convection [*Lee*, 2006; *Lee et al.*, 2005], 2) small volume partial melt starting at the top of the asthenosphere [*Karato and Jung*, 1998; *Lee*, 2006], including sheared lenses containing melt [*Kawakatsu et al.*, 2009], 3) grain size reduction in the flowing asthenosphere [*Faul and Jackson*, 2005], and 4) an anisotropy boundary where frozen lithospheric anisotropy gives way to plate motion directed asthenospheric anisotropy [*Debayle et al.*, 2005; *Plomerová et al.*, 2002]. These are all reasonable means of reducing seismic velocities with depth, and therefore are candidate mechanisms for producing a seismic signal correlated with the LAB. This underscores the complexity of the LAB in comparison to other seismic discontinuities such as the Moho (chemical, modulated by tectonics) and the mantle transition zone (controlled by temperature and pressure, mediated by volatiles). It also complicates possibilities for the cause of the seismic LAB in an orogenic setting.

[23] All of these can produce converted wave seismic signals, but of somewhat different characteristics. In regions where thermal equilibration cannot keep pace with tectonic activity, the seismic signals ascribed to the LAB can originate from zones of small volume partial melt, zones of hydration, zones of upper mantle flow, or a combination of these. The frequency dependence of signals converted at the LAB will depend on its thickness and possibly on internal structure. Since all of the possibilities mentioned above can control the location of the LAB, we hypothesize that it is feasible that velocity reductions occur at several different depths beneath any location due to different processes in regions of complex tectonics. As some of these potential sources of a seismic conversion will produce frequency dependence in the conversions, it is not surprising that the events seen in the Sp and Ps image volumes, and LAB depths inferred from long period surface waves are not always identical. Rather than attempt to associate the LAB everywhere in the western U.S. to specific physical causes, which would require encyclopedic discussion as well as considerably greater labor, here we confine our attention to measuring the LAB depth and suggesting physical causes where possible. We leave more detailed descriptions to more local studies.

[24] Almost everywhere west of the hinge line the Ps and Sp depths to the first sub-Moho velocity reduction are nearly coincident, and the two surfaces have similar structural trends, therefore we are mapping a consistent low velocity anomaly which we identify as the LAB. As we have described above, east of the hingeline we rely upon the Sp conversions for identifying deeper negative events in the Ps volume that we associate with the LAB. Where we have Rayleigh wave derived shear velocity models [*Yang et al.*, 2008; *Liu et al.*, 2011, 2012] the negative velocity gradients in the upper mantle are also coincident with the Ps and Sp conversions. To us this suggests that we are mapping the LAB in a seismic, if not rheological sense in the Rockies and Colorado Plateau, as well as

west of the hingeline. If we assume that the seismic impedance coincides spatially with a strength reduction, then the negative event is the LAB in a rheologic sense.

[25] Even with the Ps LAB chosen using Sp as a guide, the Sp LAB depths are somewhat greater, 4.0 km on average over the entire western U.S., or about 5–6% of average lithosphere thickness (Figure 2 and Tables 3 and 4). Although a relatively modest discrepancy, several possible explanations can cause this difference: 1) errors in the data processing, depth mapping, and signal identification, 2) frequency dependent signal interference and scattering effects, and 3) imperfections in the velocity model used for spatially position the data.

[26] For the first, we have tested our RF, CCP stacking, and depth mapping codes independently with synthetic data and don't believe that errors in the data processing and depth mapping can explain the LAB depth discrepancy. Depth mapping Ps and Sp receiver functions beneath individual stations using identical velocity models produces similar discrepancies between Ps and Sp estimates of LAB depth. Where the LAB is deep, as in the Rocky Mountains, crustal multiple reflections can interfere with the primary Ps conversions in this depth range. We have calculated synthetic RFs for all USArray stations using the continuity and H-κ Moho models, to exclude the possibilities that the Ps LAB events are mis-identified crustal multiples. We have also used the synthetics to identify the intracrustal multiples predicted by Crust2.0.

[27] Several types of signal interference effects arise in Sp RFs. If the Moho is shallow, the direct S and converted Sp phase can interfere, biasing the Moho estimate to greater depths. Where the upper mantle separating the Moho and LAB is on the order of or less than the converted P wavelength, the Sp phases from the Moho and LAB can interfere in the common Sp frequency band (see Figure S2 in Text S1). The interference causes the Moho to appear shallower, and the LAB to appear deeper (see Figure S2 in Text S1). This is certainly a possibility in this data set, as LAB depths are generally less than twice Moho depths west of the hingeline. Tables 1–4 show that the Sp Moho depths are less than the Ps depths, whereas Sp LAB depths are greater than Ps LAB depths, suggesting the Sp RFs signals are affected by interference. Another consideration is wavelength dependent scattering, an example of which we illustrate in Figure S2 in Text S1. A small velocity reduction in an otherwise homogeneous uppermost mantle is detectable by 0.5 Hz Ps RFs, but is undetectable by 0.2 Hz Sp RFs.

[28] To check the reasonability of our choice of LAB we turn to other geoscience information. We compared the LAB depth estimates from the receiver function images to the calculated melting temperatures and pressures of basalts [*Lee et al.*, 2009] beneath the Basin and Range, the Colorado Plateau, and Cascadia. The depth estimates from the geochemistry data generally compare well with our chosen lithosphere-asthenosphere boundary depths. For example, *Lee et al.* [2009] identify the LAB lying between 60 and 76 km in the Basin and Range, the Ps and Sp RF estimates are 60.7 $\pm$ 7.8 and 66.1 $\pm$ 9.3 km (Tables 3 and 4). Under the Colorado Plateau the RF depths are 86.2 $\pm$ 13.9 (Ps) and 92.8 $\pm$ 15.2 (Sp), with the geochemical estimates being 95–115 km.

[29] The geochemical data show a variation in the depth of melting generally greater than 30 km in each region, often at the same volcanic center. The greatest pressures (depths) often represent the onset of melting, which is likely to correspond to the bottom of a velocity gradient forming the seismically detected LAB. In the RF cross-sections (Figure 2) bright negative amplitudes below the Cascadia backarc, parts of the Basin and Range, and around the rim of the Colorado Plateau (Figures 2b and 5) have been interpreted as regions of partial melt in asthenospheric mantle from high Vp/Vs ratios [*Schmandt and Humphreys*, 2010]. LAB depths are shallow in these regions (Figure 3). In the western Colorado Plateau, isotope analysis of recent mafic volcanism led *Reid et al.* [2012] to argue that decompression melting occurs just below the seismological proxy for the LAB that we present here. To us this supports a local model of the LAB as the top of a partial melt zone around the periphery of the Colorado Plateau.

[30] Although the lithospheric thickness maps represent the LAB as a single surface (Figure 4), we emphasize that everywhere, and particularly beneath the hingeline and the Colorado Plateau and the Rocky Mountains, the negative events appear as a complex zone in depth. This can be due to imperfections in the imaging, or due to complexity in the mantle. First, where lithosphere thickness is changing rapidly, the assumptions behind the CCP method begin to break down, blurring our images and mispositioning converted events in space [*Rondenay*, 2009]. The deeper the dipping interface the more imprecise the image. Second, the available geochemical data as well as body and

surface wave tomography and receiver function images suggest that transitions in material properties can be distributed throughout a depth range at a given location. We feel that choosing a single continuous surface to represent the LAB everywhere is somewhat artificial. Presumably the LAB depths we have produced are still of use to mantle seismologists attempting to account for lithospheric travel times, and provide other earth scientists with a sense of lithospheric thickness variation.

5. Discussion

[31] We wish to emphasize an important difference between the two discontinuities that we identify in the receiver function volumes: The Moho is almost everywhere a continuous surface except in regions of convective downwelling or unusual material properties (as in the Cascadia forearc region), whereas the LAB is often not simple (Figures 2–5). The difference in the causes of the boundaries permit more spatial variation in the LAB than the Moho: The LAB exists in a much simpler chemical and mineralogical system (variations of the peridotite minerals, and eclogitized basalt) whose first order controls are temperature and pressure, i.e., properties that we expect to vary smoothly in space, and the presence of volatiles, whose spatial distribution is poorly known, but is likely locally concentrated (e.g., in the Cascadia subduction zone and backarc) or regionally (under the Colorado Plateau resulting from both melts and past dewatering during Farallon flat slab subduction). Further, depth variations in grain size and orientation, and hence anisotropy indicative of present and past directions of mantle flow and strain, can also produce seismic signals from the upper mantle. At very least, the anisotropy resulting from present mantle flow directions can be influenced by the presence of volatiles. These effects combine to produce weaker and more complicated signals in comparison to those from the Moho.

5.1. Tectonic Implications

[32] Beyond mapping the lithospheric discontinuities and measuring province wide amplitude ratios, the two lithospheric boundaries reflect tectonic processes that occurred from the mid-Mesozoic to the present. Although the western U.S. can be divided broadly into a small number of physiographic/tectonic provinces (Figures 1 and 3–5), on the largest scale Moho and the LAB depths show less correlation with physiographic province than with the approximately east-west division along the Paleozoic Cordilleran hinge-line that marked the eastern edge of the Laurasian passive margin sediments (Figures 3 and 5). The Paleozoic hingeline subsequently became the axis of the Sevier fold and thrust belt. In most of the western U.S., this change in lithospheric discontinuity depth lies several hundred kilometers west of the east-west division between positive and negative Vp and Vs anomalies in the upper 200 km of the mantle under the western orogenic belt [*Grand*, 1987, 1994; *Schmandt and Humphreys*, 2010]. Another consistent geophysical measurement is effective elastic thickness of the western U.S. [*Lowry and Pérez-Gussinye*, 2011], which shows a similar pattern to the LAB structure presented here. It increases abruptly east of the hingeline, from less than 10 km to more than 30 km from west to east, within a larger North American pattern of low elastic thickness in the diffuse plate boundary zone (10–50 km) and large elastic thickness in the cratonic interior (80–150 km) [*Audet and Burgmann*, 2011].

[33] Figure 5 illustrates the correlation between the LAB depths with volcanism (5–0 Ma) and a sample of seismicity recorded over the past 10 years. Large gradients in Moho and/or LAB depth (Figure 6) are strongly correlated with modern faulting and Late Cenozoic volcanism almost everywhere in the western U.S. The correlation of seismicity and lithospheric thickness suggests that the location of faulting is controlled by abrupt changes in integrated lithospheric strength. In particular we note the eastern side of the continental arc south of the Mendocino Triple Junction, the western and southwestern edges of the Colorado Plateau, the Cordilleran hinge-line generally, and the two sides of the Rio Grande rift. In addition to zones of seismicity and volcanism the steps in depth to the LAB along the hingeline are thought to be sites dominated by edge-convection or delamination processes, which we discuss further below.

[34] One striking feature in both the Moho depth map (Figure 3) and the LAB depth map (Figure 5) is the change in thicknesses in southern California and the correlation to earthquakes along the southern parts of the San Andreas system and the Eastern California Shear Zone (ECSZ). Like *Lekic et al.* (2011) we also find a thinned lithosphere under the Salton trough. As proposed by *Nur et al.* [1993], the Landers earthquake and associated seismicity along this fault, and the ECSZ, are indicative of a geologically young fault that is replacing an older segment of the plate bounding strike-slip system. Both seismicity and lithospheric deformation can be linked to reorganization of the

plate boundary system and pre-existing lithosphere thickness: The locus of deformation is being transferred from the bend in the southern San Andreas Fault (SAF) to the ECSZ, which is the next zone of thin lithosphere to the east. Between the east side of the Sierra Nevada and the Basin and Range is a lithospheric trough about 20 km thinner than the lithosphere to either side, with associated clustered seismicity and volcanism. Seismicity is concentrated linearly along the east side of the Sierra Nevada batholith through the Walker Lane along the edge of relatively thicker lithosphere. Where the lithosphere thins near 40°N, 118°W the zone of deformation widens to include the central Nevada seismic zone [*Hammond and Thatcher*, 2007].

[35] Volcanism younger than 5 Myr rings the Basin and Range, but relatively little young volcanism appears interior to it, despite its thin lithosphere. The Salton trough and the northeastern Basin and Range crust in front of the Wasatch front have significantly thinner crust than average, and both have thinned lithosphere. The southwestern Basin and Range stands out as its crustal thickness is considerably less than the northern Basin and Range, its LAB is shallow, and its elevation is significantly lower than the northern Basin and Range. North of the 40°N trend of thin lithosphere across the Basin and Range, the lithosphere thickens fairly regularly to the Snake River Plain.

[36] The gradients in thicknesses across the hingeline are the most obvious features of both the gradient maps of the western U.S. Moho and LAB (Figure 7). From Yellowstone south along the Wasatch front to the Cheyenne belt, around the peripheries of the Colorado Plateau and the Rio Grande rift, deformation (seismicity), volcanism in the past 5 Myr, and a change in heat flow regimes (Blackwell; http://smu.edu/geothermal/heatflow/heatflow.htm) appear at abrupt increases in LAB depth, and less abrupt increases in Moho depth. The Colorado Plateau-Wasatch Front boundary acts to localize deformation as indicated by seismicity. Between the Snake River Plain-Yellowstone system and the Wasatch front to the Cheyenne belt, recent volcanism is far less decent than further south and is highly localized (Figure 5). The edges of the physiographically defined Colorado Plateau do not match the abrupt change in depth to the LAB. South of the Cheyenne Belt the peripheries of the Colorado Plateau have been progressively invaded by magmas, with the youngest being closest to the plateau center [*Roy et al.*, 2009]. The volcanism that rings the inner plateau periphery is attributed to asthenospheric "erosion" of various types of the CP cratonic core for the past 20 Myr [*Levander et al.*, 2011; *Reid et al.*, 2012; *Roy et al.*, 2009; *van Wijk et al.*, 2010]. The association of seismicity and particularly volcanism with large negative gradients in lithospheric thickness is very noticeable on both sides of the Rio Grande rift. Recent volcanism along the trend of the Rio Grande rift extends almost as far north as the Cheyenne belt, and is clustered along either side of a zone of lithosphere that thins southward. Lithosphere structure suggests that the Rio Grande Rift extends to at least 40°N (Figures 3c and 3d).

[37] The Jemez lineament appears to be a zone of thinned lithosphere associated with the Rio Grande Rift. It extends northeast to the Raton volcanic field in New Mexico through the Rio Grande Rift, and southwestward to the southern edge of the Colorado plateau, more or less following the edges of the thinned lithosphere under the Rift and Colorado Plateau. This is in agreement with previous studies of the northeastern Jemez Lineament [*Levander et al.*, 2005; *Yuan and Dueker*, 2005] The lineament also approximately follows the Proterozoic Yavapai-Mazatzal suture [*Karlstrom and Humphreys*, 1998], further evidence that physical and/or chemical heterogeneities inherited from ancient orogenies can focus deformation in modern systems.

5.2. Convective Downwelling

[38] We note that the sites in the western U.S. where large convective downwellings have been identified are along steep gradients in lithosphere or crustal thickness: The southern Sierra Nevada [*Zandt*, 2003], the Wallowa Mountains [*Hales et al.*, 2005], the eastern edge of the Rio Grande rift [*van Wijk et al.*, 2010], and several places along the western Colorado Plateau [*Levander et al.*, 2011; *van Wijk et al.*, 2010]. All of these previously recognized locations of downwellings are present in our receiver function volumes (see auxiliary material). *Levander et al.* [2011] proposed a 3-D thermo-chemical convection process to explain lower-crustal and upper mantle delamination structures evident in both receiver functions and tomography beneath the Colorado Plateau. The dipping structure and the overlying shallow Moho signal are clearly shown in both the Ps and Sp receiver functions in Figure 2a. Further evidence from petrological data describing decompression melting processes [*Reid et al.*, 2012] supports the idea of complex 3D convection and removal of the

base of the lithosphere beneath this region. We agree that the three-dimensional heterogeneous Wallowa Mountains and southern Sierra Nevada anomalies are detachments of lithospheric instabilities due to convective processes at the edges of lithospheric or crustal thickness changes, and that there are likely others yet to be discovered.

[39] The images suggest that edge convection is active along the entire western edge of the Colorado Plateau, along parts of the Wasatch front north of the Cheyenne belt, and under parts of the western edge of the northern U.S. Rockies. If so two and three-dimensional edge convection are dominant processes in the western U.S.

6. Conclusion

[40] USArray has provided us with an outstanding data set for investigating the lithosphere in the Western U.S. Given that the entire region has been undergoing tectonic modification since the Mesozoic, we observe a large range in lithospheric thickness. To first order heat flow is correlated to lithosphere thickness. The strongest controls on lithospheric deformation in the western United States are, first, the edge of the Paleozoic passive margin, and second the age of the pre-existing lithosphere, with the Proterozoic mantle lithosphere apparently having experienced more dramatic erosion around the Colorado Plateau and in the Rio Grande rift than anywhere in the Archean province. Whether the latter is due to differences in tectonic history, or is largely the result of the more depleted Archean lithosphere being more viscous and more buoyant than the Proterozoic lithosphere is not clear, but we are inclined toward the latter view [*Jordan*, 1978]. South of the Cheyenne belt the Moho has been reset within some of the former Precambrian terranes but not always in exact congruence with erosion of mantle lithosphere. West of the hinge line both of the lithospheric discontinuities are almost everywhere mid-Cenozoic or younger, a possible exception being remnant Mesozoic Moho under parts of the northern Sierra Nevada. Away from the plate boundary, both seismicity and volcanism are associated with the physiographic/tectonic province boundaries only if they also correspond to abrupt gradients in lithospheric and/or crustal thicknesses. The one notable exception to this is the Snake River Plain-Yellowstone volcanic system whose origin has been ascribed to a plume [*Obrebski et al.*, 2011; *Schmandt et al.*, 2012]. Elsewhere abrupt gradients in Moho and lithospheric thickness are more likely to be zones of deformation and magmatism than the tectonic/physiographic boundaries. Finally the identified convective downwellings of the secondary convection system, i.e, those not directly part of Farallon plate subduction, are located at rapid gradients in lithospheric thickness, a requirement of edge-type convection. Whether all downwellings are thermochemical and three-dimensional in nature, departing from the 2-D thermal edge convection model, is not yet clear.

Acknowledgments

[41] We would like to thank Fenglin Niu, Kaijian Liu, Yongbo Zhai, Yan Xu, and Meijuan Jiang for assisting with data processing. We benefited from discussions with Cin-Ty Lee and Adrian Lenardic. The Associate Editor and two reviewers made thoughtful comments. The Sp receiver function study began as an exercise at the 2008 CIDER (Cooperative Institute for Deep Earth Research) summer school. This research was funded by Earthscope grant EAR-0844741 and EAR-0844760. AL gratefully acknowledges a Humboldt Research Prize from the Alexander von Humboldt Foundation. The Ps study was undertaken while AL was on sabbatical at the GeoForschungsZentrum Potsdam, Germany.

References

Abt, D. L., K. M. Fischer, S. W. French, H. A. Ford, H. Yuan, and B. Romanowicz (2010), North American lithospheric discontinuity structure imaged by *Ps* and *Sp* receiver functions, *J. Geophys. Res.*, *115*, B09301, doi:10.1029/2009JB006914.

Artemieva, I. M. (2009), The continental lithosphere: Reconciling thermal, seismic and petrologic data, *Lithos*, *109*, 23–46, doi:10.1016/j.lithos.2008.09.015.

Atwater, T. (1970), Implications of plate tectonics for the Cenozoic tectonic evolution of western North America, *Geol. Soc. Am. Bull.*, *81*, 3513–3536, doi:10.1130/0016-7606(1970)81[3513:IOPTFT]2.0.CO;2.

Audet, P., and R. Burgmann (2011), Dominant role of tectonic inheritance in supercontinent cycles, *Nat. Geosci.*, *4*, 184–187.

Bassin, C., G. Laske, and G. Masters (2000), The current limits of resolution for surface wave tomography in North America, *Eos Trans. AGU*, *81*(48), Fall Meet. Suppl., Abstract S12A-03.

Blakely, R. J., T. M. Brocher, and R. E. Wells (2005), Subduction-zone magnetic anomalies and implications for hydrated forearc mantle, *Geology*, *33*, 445–448, doi:10.1130/G21447.1.

Bostock, M. G., S. Rondenay, and D. S. Schragge (2001), Multiparameter two-dimensional version of scattered teleseismic body waves: 1. Theory for oblique incidence, *J. Geophys. Res.*, *106*, 30,771–30,782, doi:10.1029/2001JB000330.

Bostock, M. G., R. D. Hyndman, S. Rondenay, and S. M. Peacock (2002), An inverted continental Moho and serpentinization of the forearc mantle, *Nature*, *417*, 536–538, doi:10.1038/417536a.

Brocher, T. M., T. Parons, A. M. Tréhu, C. M. Snelson, and M. A. Fischer (2003), Seismic evidence for widespread serpentinized forearc upper mantle along the Cascadia Margin, *Geology*, *31*, 267–270, doi:10.1130/0091-7613(2003)031<0267:SEFWSF>2.0.CO;2.

Buehler, J., and M. Shearer (2010), Pn tomography of the western United States using USArray, *J. Geophys. Res.*, *115*, B09315, doi:10.1029/2009JB006874.

Chapman, D. S., and H. N. Pollack (1977), Regional geotherms and lithospheric thickness, *Geology*, *5*, 265–268, doi:10.1130/0091-7613(1977)5<265:RGALT>2.0.CO;2.

Cook, F. A., D. J. White, A. G. Jones, D. W. S. Eaton, J. Hall, and R. M. Clowes (2010), How the crust meets the mantle: Lithoprobe perspectives on the Mohorovicic discontinuity and crust-mantle transition, *Can. J. Earth Sci.*, *47*, 315–351.

Debayle, E., B. L. N. Kennett, and K. Priestley (2005), Global azimuthal anisotropy and unique plate motion-deformation of Australia, *Nature*, *433*, 509–512, doi:10.1038/nature03247.

DeCelles, G. (2004), Late Jurassic to Eocene evolution of the Cordilleran thrust belt and foreland basin system, western U.S., *Am. J. Sci.*, *304*, 105–168, doi:10.2475/ajs.304.2.105.

Dueker, K. G., and A. F. Sheehan (1997), Mantle discontinuity structure form midpoint stacks of converted P to S waves across the Yellowstone hotspot track, *J. Geophys. Res.*, *102*, 8313–8327, doi:10.1029/96JB03857.

Eaton, D. W., F. A. Darbyshire, R. L. Evans, H. Grutter, and A. G. Jones (2009), The elusive lithosphere-asthenosphere boundary (LAB) beneath craton, *Lithos*, *109*, 1–22, doi:10.1016/j.lithos.2008.05.009.

Farra, V., and L. P. Vinnik (2000), Upper mantle stratification by P and S receiver functions, *Geophys. J. Int.*, *141*, 699–712, doi:10.1046/j.1365-246x.2000.00118.x.

Faul, U., and I. Jackson (2005), The seismological signature of temperature and grain size variations in the upper mantle, *Earth Planet. Sci. Lett.*, *234*, 119–134, doi:10.1016/j.epsl.2005.02.008.

Fischer, K. M., H. A. Ford, D. L. Abt, and C. A. Rychert (2010), The lithosphere-asthenosphere boundary, *Annu. Rev. Earth Planet. Sci.*, *38*, 551–575, doi:10.1146/annurev-earth-040809-152438.

Forsyth, D. W., and C. J. Rau (2009), Isabella anomaly, lithospheric drip, delamination or fragment of the Farallon plate, *Eos Trans. AGU*, *90*(52), Fall Meet. Suppl., Abstract U33C-06.

Gilbert, H. (2012), Crustal structure and signatures of recent tectonism influenced by ancient terranes in the western United States, *Geosphere*, *8*, 141–157, doi:10.1130/GES00720.1.

Godfrey, N. J., B. C. Beaudoin, S. L. Klemperer, A. Levander, J. H. Luetgert, A. S. Meltzer, W. D. Mooney, and A. M. Trehu (1997), Ophiolitic basement to the Great Valley forearc basin, California, from seismic and gravity data: Implications for crustal growth at the North American continental margin, *Geol. Soc. Am. Bull.*, *109*, 1536–1562, doi:10.1130/0016-7606(1997)109<1536:OBTTGV>2.3.CO;2.

Gordon, R. G. (1998), The plate tectonic approximation: Plate nonrigidity, diffuse plate boundaries, and global plate reconstructions, *Annu. Rev. Earth Planet. Sci.*, *26*, 615–642, doi:10.1146/annurev.earth.26.1.615.

Gorman, A. R., et al. (2002), Deep Probe—Imaging the roots of western North America, *Can. J. Earth Sci.*, *39*, 375–398, doi:10.1139/e01-064.

Grand, S. P. (1987), Tomographic inversion for shear velocity beneath the North American Plate, *J. Geophys. Res.*, *92*, 14,065–14,090, doi:10.1029/JB092iB13p14065.

Grand, S. P. (1994), Mantle shear structure beneath the Americas and surrounding oceans, *J. Geophys. Res.*, *99*, 11,591–11,621, doi:10.1029/94JB00042.

Griffin, W. L., and S. Y. O'Reilly (1987), Is the Moho the crust–mantle boundary?, *Geology*, *15*, 241–244, doi:10.1130/0091-7613(1987)15<241:ITCMTC>2.0.CO;2.

Hales, T. C., D. L. Abt, E. D. Humphreys, and J. J. Roering (2005), A lithospheric instability origin for Columbia River flood basalts and Wallowa Mountains uplift in northeast Oregon, *Nature*, *438*, 842–845, doi:10.1038/nature04313.

Hammond, W. C., and W. Thatcher (2007), Crustal deformation across the Sierra Nevada, northern Walker Lane, Basin and Range transition, western United States measured with GPS, 2000–2004, *J. Geophys. Res.*, *112*, B05411, doi:10.1029/2006JB004625.

Henstock, T. J., A. Levander, C. M. Snelson, G. R. Keller, K. C. Miller, S. H. Harder, A. R. Gorman, R. M. Clowes, M. J. A. Burianyk, and E. D. Humphreys (1998), Probing the Archean and Proterozoic lithosphere of western North America, *GSA Today*, *8*, 1–17.

Hirth, G., and D. L. Kohlstedt (1996), Water in the oceanic upper mantle: Implications for rheology, melt extraction and the evolution of the lithosphere, *Earth Planet. Sci. Lett.*, *144*, 93–108, doi:10.1016/0012-821X(96)00154-9.

Holbrook, W. S. (1990), The crustal structure of the northwestern Basin and Range, *J. Geophys. Res.*, *95*, 21,843–21,869, doi:10.1029/JB095iB13p21843.

Humphreys, E. D. (1995), Post-Laramide removal of the Farallon slab, western United States, *Geology*, *23*, 987–990, doi:10.1130/0091-7613(1995)023<0987:PLROTF>2.3.CO;2.

Humphreys, E. D., E. Hessler, K. G. Dueker, G. L. Farmer, E. Erslev, and T. Atwater (2003), How Laramide-age hydration of North American lithosphere by the Farallon slab controlled subsequent activity in the western United States, *Int. Geol. Rev.*, *45*, 575–595, doi:10.2747/0020-6814.45.7.575.

Hyndman, R. D., C. A. Currie, and S. Mazzotti (2005), Subduction zone backarcs, mobile belts, and orogenic heat, *GSA Today*, *15*, 4–10.

Jarchow, C. M., and G. A. Thompson (1989), The nature of the Mohorovicic discontinuity, *Annu. Rev. Earth Planet. Sci.*, *17*, 475–506, doi:10.1146/annurev.ea.17.050189.002355.

Jordan, T. H. (1978), Composition and development of the continental tectosphere, *Nature*, *274*, 544–548, doi:10.1038/274544a0.

Karato, S., and H. Jung (1998), Water, partial melting and the origin of the seismic low velocity and high attenuations zone in the upper mantle, *Earth Planet. Sci. Lett.*, *157*, 193–207, doi:10.1016/S0012-821X(98)00034-X.

Karlstrom, K. E., and E. D. Humphreys (1998), Persistent influence of Proterozoic accretionary boundaries in the tectonic evolution of southwestern North America: Interaction of cratonic grain and mantle modification events, in *Mountain Geology*, vol. 33, *Lithospheric Structure and Evolution of the Rocky Mountains*, edited by K. E. Karlstrom, pp. 161–179, Geol. Soc. of Am., Boulder, Colo.

Kawakatsu, H., P. Kumar, Y. Takei, M. Shinohara, T. Kanazawa, E. Araki, and K. Suyehiro (2009), Seismic evidence for sharp lithospheric-asthenosphere boundaries of oceanic plates, *Science*, *324*, 324–327.

Kennett, B. L. N., E. R. Engdahl, and R. Buland (1995), Constraints on seismic velocities in the Earth from travel times, *Geophys. J. Int.*, *122*, 108–124, doi:10.1111/j.1365-246X.1995.tb03540.x.

Klemperer, S. L., T. A. Hauge, E. C. Hauser, J. E. Oliver, and C. J. Potter (1986), The Moho in the northern Basin and Range province, Nevada, along the COCORP 40°N seismic reflection transect, *Geol. Soc. Am. Bull.*, *97*, 603–618, doi:10.1130/0016-7606(1986)97<603:TMITNB>2.0.CO;2.

Langston, C. A. (1977), Corvallis, Oregon, crustal and upper mantle receiver structure from teleseismic P and S waves, *Bull. Seismol. Soc. Am.*, *67*, 713–724.

Larkin, S. P., A. Levander, T. J. Henstock, and S. Pullammanappallil (1997), Is the Moho flat? Seismic evidence for a rough crust-mantle interface beneath the northern Basin and Range, *Geology*, *25*, 451–454, doi:10.1130/0091-7613(1997)025<0451:ITMFSE>2.3.CO;2.

Lee, C.-T. A. (2006), Geochemical/petrologic constraints on the origin of cratonic mantle, in *Archean Geodynamics and Environments*, *Geophys. Monogr. Ser.*, vol. 164, edited by K. Benn, J.-C. Mareschal, and K. C. Condie, pp. 89–114, AGU, Washington, D. C., doi:10.1029/164GM08.

Lee, C.-T. A., A. Lenardic, C. M. Cooper, F. Niu, and A. Levander (2005), The role of chemical boundary layers in regulating the thickness of continental and oceanic thermal boundary layers, *Earth Planet. Sci. Lett.*, *230*, 379–395, doi:10.1016/j.epsl.2004.11.019.

Lee, C.-T. A., P. Luffi, T. Plank, H. Dalton, and W. P. Leeman (2009), Constraints on the depths and temperatures of basaltic magma generation on Earth and other terrestrial planets using new thermobarometers for mafic magmas, *Earth Planet. Sci. Lett.*, *279*, 20–33, doi:10.1016/j.epsl.2008.12.020.

Lekic, V., S. W. French, and K. M. Fischer (2011), Lithospheric thinning beneath rifted regions of Southern California, *Science*, *334*, 783–787, doi:10.1126/science.1208898.

Levander, A., C. A. Zelt, and M. B. Magnani (2005), Crust and upper mantle velocity structure of the southern Rocky Mountains from the Jemez Lineament to the Cheyenne Belt, in *The Rocky Mountain Region—An Evolving Lithosphere: Tectonics, Geochemistry, and Geophysics*, *Geophys. Monogr. Ser.*, vol. 154, edited by K. E. Kalstrom and G. R. Keller, pp. 293–308, AGU, Washington, D. C., doi:10.1029/154GM22.

Levander, A., B. Schmandt, M. S. Miller, K. E. Karlstrom, R. S. Crow, K. Liu, C.-T. A. Lee, and E. Humphreys (2011), Continuing Colorado plateau uplift by delamination-style convective lithospheric downwelling, *Nature*, *472*, 461–465, doi:10.1038/nature10001.

Li, X., X. Yuan, and R. Kind (2007), The lithosphere-asthenosphere boundary beneath the western United States, *Geophys. J. Int.*, *170*, 700–710, doi:10.1111/j.1365-246X.2007.03428.x.

Ligorria, J. P., and C. J. Ammon (1999), Iterative deconvolution and receiver-function estimation, *Bull. Seismol. Soc. Am.*, *89*, 1395–1400.

Liu, K., A. Levander, F. Niu, and M. S. Miller (2011), Imaging crustal and upper mantle structure beneath the Colorado Plateau using finite frequency Rayleigh wave tomography, *Geochem. Geophys. Geosyst.*, *12*, Q07001, doi:10.1029/2011GC003611.

Liu, K., A. Levander, Y. Zhai, R. Poritt, and R. A. Allen (2012), Asthenospheric flow and lithospheric evolution near the Mendocino triple junction, *Earth Planet. Sci. Lett.*, *323–324*, 60–71, doi:10.1016/j.epsl.2012.01.020.

Lonsdale, P. (1991), Structural patterns of the Pacific floor offshore Peninsular California, *AAPG Mem.*, *47*, 87–125.

Lowry, A. R., and M. Pérez-Gussinye (2011), The role of crustal quartz in controlling Cordilleran deformation, *Nature*, *471*, 353–357, doi:10.1038/nature09912.

Meltzer, A. S., and A. Levander (1991), Deep crustal reflection profiling offshore southern central California, *J. Geophys. Res.*, *96*, 6475–6491, doi:10.1029/91JB00120.

Miller, M. S., and D. W. Eaton (2010), Formation of cratonic mantle keels by arc accretion: Evidence from S receiver functions, *Geophys. Res. Lett.*, *37*, L18305, doi:10.1029/2010GL044366.

Mooney, W. D., G. Laske, and G. Masters (1998), Crust 5.1: A global crustal model at 5 × 5 degrees, *J. Geophys. Res.*, *103*, 727–747, doi:10.1029/97JB02122.

Nur, A., H. Ron, and G. C. Beroza (1993), The nature of the Landers-Mojave earthquake line, *Science*, *261*, 201–203, doi:10.1126/science.261.5118.201.

Obrebski, M., R. M. Allen, F. Pollitz, and S.-H. Hung (2011), Lithosphere-asthenosphere interaction beneath the western United States from the joint inversion of body-wave traveltimes and surface-wave phase velocities, *Geophys. J. Int.*, *185*, 1003–1021, doi:10.1111/j.1365-246X.2011.04990.x.

Parsons, T., J. McCarthy, W. M. Koehler, C. J. Ammon, H. M. Benz, J. A. Hole, and E. E. Criley (1996), Crustal structure of the Colorado Plateau, Arizona: Application of new long-offset seismic data analysis techniques, *J. Geophys. Res.*, *101*, 11,173–11,194, doi:10.1029/95JB03742.

Plomerová, J., D. Kouba, and V. Babuska (2002), Mapping the lithosphere-asthenosphere boundary through changes in surface-wave anisotropy, *Tectonophysics*, *358*, 175–185, doi:10.1016/S0040-1951(02)00423-7.

Reid, M. R., R. A. Bouchet, J. Blichert-Toft, A. Levander, K. Liu, M. S. Miller, and F. C. Ramos (2012), Melting under the Colorado Plateau, USA, *Geology*, *40*, 387–390, doi:10.1130/G32619.1.

Robinson, E. A., and S. Treitel (1980), *Geophysical Signal Analysis*, 466 pp., Prentice-Hall, Englewood Cliffs, N. J.

Rondenay, S. (2009), Upper mantle imaging with array recordings of converted and scattered teleseismic waves, *Surv. Geophys.*, *30*, 377–405, doi:10.1007/s10712-009-9071-5.

Rondenay, S., M. G. Bostock, and J. Shragge (2001), Multiparameter two-dimensional inversion of scattered teleseismic body waves: 3. Application to the Cascadia 1993 data set, *J. Geophys. Res.*, *106*, 30,795–30,807, doi:10.1029/2000JB000039.

Roy, M., T. H. Jordan, and J. Pederson (2009), Colorado Plateau magmatism and uplift by warming of heterogeneous lithosphere, *Nature*, *459*, 978–982, doi:10.1038/nature08052.

Rychert, C. A., and M. Shearer (2009), A global view of the lithosphere-asthenosphere boundary, *Science*, *324*, 495–498, doi:10.1126/science.1169754.

Rychert, C. A., S. Rondenay, and K. M. Fischer (2007), *P*-to-*S* and *S*-to-*P* imaging of a sharp lithosphere-asthenosphere boundary beneath eastern North America, *J. Geophys. Res.*, *112*, B08314, doi:10.1029/2006JB004619.

Schmandt, B., and E. D. Humphreys (2010), Complex subduction and small-scale convection revealed by body-wave tomography of the western United States upper mantle, *Earth Planet. Sci. Lett.*, *297*, 435–445, doi:10.1016/j.epsl.2010.06.047.

Schmandt, B., and E. D. Humphreys (2011), Seismically imaged relict slab from the 55 Ma Siletzia accretion to the northwest United States, *Geology*, *39*, 175–178, doi:10.1130/G31558.1.

Schmandt, B., K. Dueker, E. D. Humphreys, and S. Hansen (2012), Hot mantle upwelling across 1 the 660 beneath Yellowstone, *Earth Planet. Sci. Lett.*, *331–332*, 224–236, doi:10.1016/j.epsl.2012.03.025.

Sleep, N. H. (2005), Evolution of the continental lithosphere, *Annu. Rev. Earth Planet. Sci.*, *33*, 369–393, doi:10.1146/annurev.earth.33.092203.122643.

Smith, R. B., W. C. Nagy, K. A. Julander, J. J. Viveiros, C. A. Barker, and D. G. Gants (1989), Geophysical and tectonic framework of the eastern Basin and Range-Colorado Plateau-Rocky Mountain transition, in *Geophysical Framework of the Continental United States*, edited by L. C. Pakiser and W. D. Mooney, *Mem. Geol. Soc. Am.*, *172*, 205–233.

Snelson, C. M., T. J. Henstock, G. R. Keller, K. M. Miller, and A. Levander (1998), Crust and uppermost mantle structure along the DeepProbe seismic profile, *Rocky Mt. Geol.*, *33*, 181–198.

van Wijk, J. W., W. S. Baldridge, J. van Hunen, S. Goes, R. Aster, D. D. Coblentz, S. P. Grand, and J. Ni (2010), Small-scale convection at the edge of the Colorado Plateau: Implications for topography, magmatism, and evolution of Proterozoic lithosphere, *Geology*, *38*, 611–614, doi:10.1130/G31031.1.

Vinnik, L. P. (1977), Detection of waves converted from P to SV in the mantle, *Phys. Earth Planet. Inter.*, *15*, 39–45, doi:10.1016/0031-9201(77)90008-5.

Yang, Y., M. H. Ritzwoller, F. Lin, M. P. Moschetti, and N. M. Shapiro (2008), Structure of the crust and uppermost mantle beneath the western United States revealed by ambient noise and earthquake tomography, *J. Geophys. Res.*, *113*, B12310, doi:10.1029/2008JB005833.

Yuan, H., and K. Dueker (2005), Upper mantle tomographic Vp and Vs images of the Rocky Mountains in Wyoming, Colorado, and New Mexico: Evidence for a thick heterogeneous lithosphere, in *The Rocky Mountains: An Evolving Lithosphere*, *Geophys. Monogr. Ser.*, vol. 154, edited by K. Karstrom and G. R. Keller, pp. 329–345, AGU, Washington, D. C., doi:10.1029/154GM25

Yuan, X., R. Kind, X. Li, and R. Wang (2006), The *S* receiver functions: Synthetics and data example, *Geophys. J. Int.*, *165*, 555–564, doi:10.1111/j.1365-246X.2006.02885.x.

Zandt, G. (2003), The sourthern Sierra Nevada drip and the mantle wind direction beneath the southwestern United States, *Int. Geol. Rev.*, *45*, 213–224, doi:10.2747/0020-6814.45.3.213.

Zandt, G., and E. D. Humphreys (2008), Toroidal flow through the western U.S. slab window, *Geology*, *36*, 295–298, doi:10.1130/G24611A.1.

Zandt, G., H. J. Gilbert, T. J. Owens, M. Ducea, J. Saleeby, and C. H. Jones (2004), Active foundering of a continental arc root beneath the southern Sierra Nevada, California, *Nature*, *431*, 41–46, doi:10.1038/nature02847.

Zhu, L., and H. Kanamori (2000), Moho depth variation in southern California from teleseismic receiver functions, *J. Geophys. Res.*, *105*(B2), 2969–2980.